A Q-Band Free-Space Characterization of Carbon Nanotube Composites

Ahmed M. Hassan, *Member, IEEE*, Jan Obrzut, *Member, IEEE*, and Edward J. Garboczi

***Abstract*— We present a free-space measurement technique for nondestructive noncontact electrical and dielectric characterization of nanocarbon composites in the Q-band frequency range of 30–50 GHz. The experimental system and error correction model accurately reconstruct the conductivity of composite materials that are either thicker than the wave penetration depth, and therefore exhibit negligible microwave transmission (less than −40 dB), or thinner than the wave penetration depth and, therefore, exhibit significant microwave transmission. This error correction model implements a fixed wave propagation distance between antennas and corrects the complex scattering parameters of the specimen from two references, an air slab having geometrical propagation length equal to that of the specimen under test, and a metallic conductor, such as an aluminum plate. Experimental results were validated by reconstructing the relative dielectric permittivity of known dielectric materials and then used to determine the conductivity of nanocarbon composite laminates. This error correction model can simplify routine characterization of thin conducting laminates to just one measurement of scattering parameters, making the method attractive for research, development, and for quality control in the manufacturing environment.**

***Index Terms*— Conducting nanocarbon composites, error correction, free-space measurement, microwave metrology, noncontact nondestructive measurements.**

I. Introduction

THE exceptional properties of carbon nanotubes (CNTs) have led to their incorporation as additives in a wide range of composite materials suitable for electromagnetic interference shielding packages, sporting goods, wind turbine blades, hulls for maritime security boats, self-cleaning textiles, electrostatic-assisted painting inks, flame retardant composites, and many other applications in the aerospace and automotive industries [1]–[3]. The spatial dispersion of CNTs inside the composite considerably changes the dielectric properties and effective electrical and thermal conductivities that often correlate directly with the mechanical strength [2]–[4]. There is a strong need for an accurate nondestructive evaluation (NDE) technique for the online monitoring of the dispersion of CNTs in a composite, as they are being fabricated, with minimal disturbance to the fabrication process. Cavity measurements can provide high accuracy in retrieving the dielectric properties of the composite, but they are limited to materials with moderate resonance damping (conductivity) characteristics [5], [6]. Also, resonant techniques operating on evanescent near-fields are highly nonlinear with respect to the location of the specimen. Moreover, cavity methods are rather difficult to implement in situations where the speed and simplicity of operation must be combined with complete noninvasiveness to ensure that the continuous manufacturing process of the composites is not affected. From the manufacturing viewpoint, free-space evaluation of these dielectric properties is attractive since they are nondestructive, noncontact, and require minimal sample preparation. Therefore, in this paper, we opted for free-space measurements as the optimal method for the online monitoring of CNT composites.

Several free-space systems for dielectric characterization have been previously proposed [7]–[30]. Smith *et al.* [7] developed a free-space microwave system operating between 2 and 18 GHz for the characterization of radar absorbing materials. Ghodgaonkar *et al.* [8], Umari *et al.* [9], and Varadan *et al.* [10] developed a free-space microwave system with a frequency range of operation from 5.85 to 40 GHz. Measurements adapting oblique incident waves [9] and operating at different temperatures [10], [11] have also been proposed. At higher frequencies, several free-space systems for dielectric characterization have been demonstrated, operating in the V-band from 40 to 90 GHz [12], W-band from 75 to 110 GHz [13]–[17], from 30 to 250 GHz in [18], and from 18 to 760 GHz in [19]. Recently, the frequency range from 220 to 330 GHz has received rising interest [20], [21]. Tosaka *et al.* [20] tested both a time-domain spectroscopy system and a vector network analyzer (VNA) system, to reconstruct the dielectric permittivity of unknown materials, in the same frequency band of 220–330 GHz. Both systems were found to yield comparable results and the advantages and limitations of each system were highlighted [20]. Kim *et al.* [21] also implemented a 220–330 GHz free-space measurement system that can reconstruct the dielectric permittivity of unknown dielectrics without

Manuscript received November 25, 2015; revised April 24, 2016 and August 19, 2016; accepted August 20, 2016. Date of publication September 19, 2016; date of current version November 3, 2016. This work was supported in part by the National Institute of Standards and Technology (NIST) Project "Carbon Nanocomposite Manufacturing: Processing, Properties, Performance" and in part by the NIST Project "Multi-Scale Computational Modeling of Carbon Nanostructure Composites" under Grant 70NANB15H285.

A. M. Hassan is with the Department of Computer Science and Electrical Engineering, University of Missouri–Kansas City, Kansas City, MO 64110 USA (e-mail: hassanam@umkc.edu).

J. Obrzut is with the Material Measurement Laboratory, Materials Science and Engineering Division, National Institute of Standards and Technology (NIST), Gaithersburg, MD 20899 USA (e-mail: jan.obrzut@nist.gov).

E. J. Garboczi is with the Material Measurement Laboratory, Applied Chemicals and Materials Division, National Institute of Standards and Technology (NIST), Boulder, CO 80305 USA (e-mail: edward.garboczi@nist.gov).

Color versions of one or more of the figures in this paper are available online at http://ieeexplore.ieee.org.

Digital Object Identifier 10.1109/TMTT.2016.2603500

the prior knowledge of the dielectric thickness. Free-space terahertz characterization of multiwalled CNT (MWCNT) papers, in the frequency range 50–370 GHz, was also reported in [22].

Free space systems require rather elaborate error correction/calibration procedures to account for the mismatch between the cables and the antennas, the propagation of the waves from the transmitting antenna to the specimen, and the propagation of the waves from the specimen to the receiving antenna. Moreover, the reference planes need to be moved from the ports of the antennas to the interfaces of the specimen. To account for these distortions/errors, several calibration procedures have been developed that involve changing the distance between the antennas, moving the specimen to multiple locations, and/or measuring the scattering parameters of multiple references. One of the commonly used error correction procedures is the *Thru*, *Reflect*, *Line* (TRL) calibration technique [23]. The main challenge in TRL is phase reconstruction after the wave propagation distance between antennas is changed in the line standard, which disturbs alignment and coupling between antennas [23].

In the *Thru*, *Reflect*, *Match* calibration technique, the *Thru* and the *Reflect* standards are the same as in the TRL calibration technique [23], [24]. However, instead of the *Line* standard, a *Match* standard is realized by placing a radar-absorbent material layer between the two antennas that absorbs all the incident waves with negligible reflection and transmission [23], [24]. Although several radar-absorbent reference materials have been identified, they operate only in a narrow frequency range, and a broadband absorber is still difficult to achieve [23], [24].

In comparison, the *Line*, *Network*, *Network* (LNN) calibration technique does not employ corrections from *Reflect* or *Match* standards [25]. In their place, this methodology defines the calibration planes from scattering parameters after shifting the specimen position twice with an equal distance Δx between antennas at fixed position. This leads to four measurements: one *Thru* and two *Network* measurements, which are required to complete two port calibration procedures, plus another measurement at yet another location to characterize the specimen. Similar procedures employing *Line*, *Reflect*, *Reflect* (LRR) measurements can be applied to microwave nontransparent specimens with negligible transmission through the specimen [26]. Such measurements with specimen movement to specific locations between antennas are time consuming and difficult to implement in a high throughput manufacturing line. Nevertheless, the LNN error correction procedure accurately defines the calibration planes and is commonly used in the research and development environment.

In this paper, we present a noncontact free-space experimental system designed primarily for nondestructive characterization and quality control of nanocarbon composite materials. Microwave measurements of scattering parameters in the Q-band, which is defined to be between 30 and 50 GHz, provides a considerable amount of information about the material electrical and dielectric characteristics. Being a coherent technique, it is capable of reconstructing both the real and imaginary parts of the complex dielectric permittivity constant, which can be related to the dispersion of the CNTs in the composite. Our error correction procedure implements a fixed wave propagation distance between antennas and the measurement of the complex scattering parameters from only two references, *Line* and *Reflect*. The *Line* reference is implemented as an *air slab* having a geometrical propagation length equal to that of the specimen under test. The second reference, *Reflect*, involves a reflection measurement from a known *metallic conductor*, such as an aluminum plate. We show that the *Line, Reflect* (LR) error correction procedure is sufficient to reconstruct materials properties without ambiguity. Moreover, the simplicity of the technique makes it attractive for NDE and quality control in the manufacturing environment.

Bartley and Begley [23] developed the gated reflect line (GRL) calibration in the X-band which employed similar references as our proposed LR calibration. However, the fundamental difference between the GRL and our proposed LR method is that the GRL method explicitly calculates the elements of the error matrices that describe the mismatch between the cables and the antennas and the propagation of the waves from the antennas to the material under test (MUT). In this paper, we develop an alternative calibration method that extracts the calibrated response of the MUT, without calculating the explicit value of these error matrices, using a different time gating procedure and a different system of equations. Moreover, we develop the error-correction/calibration technique to accommodate both low loss and lossy MUTs as wells as MUTs with a wide range of thicknesses as detailed in the following sections.

Some of our preliminary results were presented in the conference paper [27]. However, in this paper, we consider more samples, we expand significantly on the theoretical foundation of the error-correction procedure, we present the error sensitivity analysis, and more importantly we add the case of a nontransparent sample with negligible transmission.

This paper is arranged as follows. In Section II, we describe our calibration or error correction model and in Section III, we describe the experimental setup and the measurements obtained. Finally, in Sections IV and V, we detail the uncertainty analysis and the conclusions, respectively.

II. Error Correction Model

A. Scattering Parameters Calibration

A sketch of the experimental setup is shown in Fig. 1. The coaxial ports in Fig. 1 are connected to a VNA, which acts as the source and receiver of the microwave signal. Experimentally, we measure the complex scattering parameters of the MUT, which we labeled as the *transfer* scattering parameters $\{T_{11}, T_{21}, T_{22}, T_{12}\}$. These scattering parameters are referenced at coaxial ports 1 and 2. Therefore, they are different from those that correspond to the MUT referenced at calibration planes, interfaces 1 and 2 (Fig. 1). To account for errors resulting from the wave propagation through antennas A and B, and the wave propagation in free space between the antennas and interfaces 1 and 2 of the MUT, two reference measurements are performed using standards with known propagation characteristics. The *Line* reference represents the scattering parameters of AIR, $\{L_{11}, L_{21}, L_{22}, L_{12}\}$, which

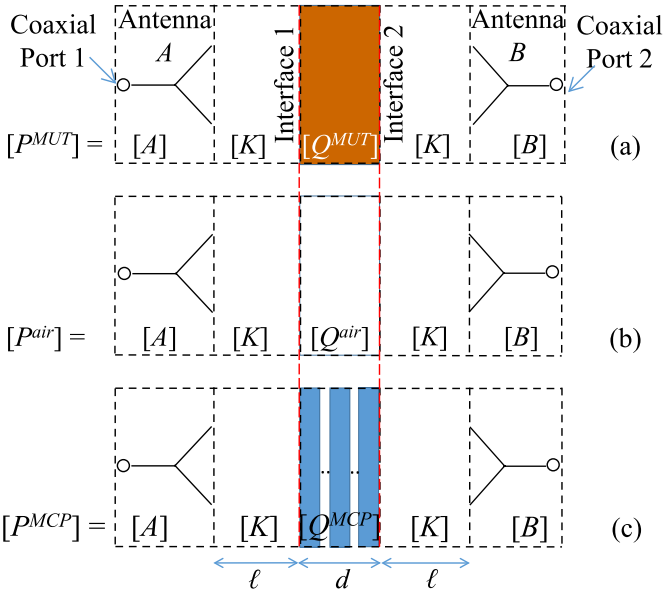

Fig. 1. Schematic of the experimental setup showing the different measurements required for the error correction procedure. (a) Specimen (MUT). (b) *Line* (AIR). (c) *Reflect* (MCP) metallic conductor plate.

account for the propagation in free space between antennas and interfaces 1 and 2. *Reflect* represents the scattering parameters of the MCP, $\{M_{11}, M_{21}, M_{22}, M_{12}\}$, which normalizes the reflections. To facilitate the derivation of the free space LR error correction terms, we express the measured scattering parameters in the form of transfer matrices $\mathbf{P}^{\mathrm{MUT}}$, $\mathbf{P}^{\mathrm{AIR}}$, and $\mathbf{P}^{\mathrm{MCP}}$ as follows:

$$\mathbf{P}^{\mathrm{MUT}} = \begin{bmatrix} P_{11}^{\mathrm{MUT}} & P_{12}^{\mathrm{MUT}} \\ P_{21}^{\mathrm{MUT}} & P_{22}^{\mathrm{MUT}} \end{bmatrix} = \begin{bmatrix} T_{21}^{-1} & -T_{21}^{-1}T_{22} \\ T_{21}^{-1}T_{11} & T_{12} - T_{11}T_{21}^{-1}T_{22} \end{bmatrix} \quad (1)$$

$$\mathbf{P}^{\mathrm{AIR}} = \begin{bmatrix} P_{11}^{\mathrm{AIR}} & P_{12}^{\mathrm{AIR}} \\ P_{21}^{\mathrm{AIR}} & P_{22}^{\mathrm{AIR}} \end{bmatrix} = \begin{bmatrix} L_{21}^{-1} & -L_{21}^{-1}L_{22} \\ L_{21}^{-1}L_{11} & L_{12} - L_{11}L_{21}^{-1}L_{22} \end{bmatrix} \quad (2)$$

$$\mathbf{P}^{\mathrm{MCP}} = \begin{bmatrix} P_{11}^{\mathrm{MCP}} & P_{12}^{\mathrm{MCP}} \\ P_{21}^{\mathrm{MCP}} & P_{22}^{\mathrm{MCP}} \end{bmatrix} = \begin{bmatrix} M_{21}^{-1} & -M_{21}^{-1}M_{22} \\ M_{21}^{-1}T_{11} & M_{12} - M_{11}M_{21}^{-1}M_{22} \end{bmatrix}. \quad (3)$$

Measurements of $\mathbf{P}^{\mathrm{MUT}}$, $\mathbf{P}^{\mathrm{AIR}}$, and $\mathbf{P}^{\mathrm{MCP}}$ given by (1)–(3) can be expressed as the multiplication of the following transfer matrices to account for the response from uncorrected components of the microwave network [25]:

$$\mathbf{P}^{\mathrm{MUT}} = \mathbf{A}\mathbf{K}\mathbf{Q}^{\mathrm{MUT}}\mathbf{K}\mathbf{B} \quad (4a)$$

$$\mathbf{P}^{\mathrm{AIR}} = \mathbf{A}\mathbf{K}\mathbf{Q}^{\mathrm{AIR}}\mathbf{K}\mathbf{B} \quad (4b)$$

$$\mathbf{P}^{\mathrm{MCP}} = \mathbf{A}\mathbf{K}\mathbf{Q}^{\mathrm{MCP}}\mathbf{K}\mathbf{B}. \quad (4c)$$

Matrices $\mathbf{A}$ and $\mathbf{B}$ account for the response from antennas A and B, the transfer matrix $\mathbf{K}$, accounts for propagation from antennas A and B to MUT, and the MUT response is represented by the matrix $\mathbf{Q}^{\mathrm{MUT}}$. Similarly, measurements (2) and (3), $\mathbf{P}^{\mathrm{AIR}}$ and $\mathbf{P}^{\mathrm{MCP}}$, can be expressed by substituting in (4a) $\mathbf{Q}^{\mathrm{AIR}}$ and $\mathbf{Q}^{\mathrm{MCP}}$, instead of $\mathbf{Q}^{\mathrm{MUT}}$, as shown in (4b) and (4c), respectively. The goal of the calibration is to extract the transfer matrix $\mathbf{Q}^{\mathrm{MUT}}$, from the measurements $\mathbf{P}^{\mathrm{MUT}}$, $\mathbf{P}^{\mathrm{AIR}}$, and $\mathbf{P}^{\mathrm{MCP}}$. The elements of the transfer matrix of antenna A are $\{A_{11}, A_{12}, A_{21}, A_{22}\}$ and the elements of the transfer matrix of antenna B are $\{B_{11}, B_{12}, B_{21}, B_{22}\}$. The propagation from antenna A to the MUT is given by the transfer matrix $\mathbf{K}$, which can be expressed as [31]

$$\mathbf{K} = \begin{bmatrix} e^{\gamma_a \ell} & 0 \\ 0 & e^{-\gamma_a \ell} \end{bmatrix} = \begin{bmatrix} k & 0 \\ 0 & k^{-1} \end{bmatrix} \quad (5)$$

where γ_a is the complex propagation constant of the waves as they travel between a distance ℓ between the antennas and the MUT and $k = e^{\gamma_a \ell}$ (see Fig. 1). Without loss of generality, it is assumed that the MUT is equidistant between the two antennas and, therefore, the same transfer matrix $\mathbf{K}$ is added to (4a)–(4c) to account for the propagation of waves from the MUT to antenna B. If in the measurement system the MUT is not equidistant between the two antennas, (1)–(4) can be still used as this shift from the equidistant position is incorporated in the transfer matrices of the antennas $\mathbf{A}$ and $\mathbf{B}$. The corrected transfer matrix $\mathbf{Q}^{\mathrm{MUT}}$, where the MUT response is embedded, can be expressed as follows [31]:

$$\mathbf{Q}^{\mathrm{MUT}} = \begin{bmatrix} q_{11} & q_{12} \\ q_{21} & q_{22} \end{bmatrix} = \begin{bmatrix} \left(S_{21}^{\mathrm{MUT}}\right)^{-1} & -\left(S_{21}^{\mathrm{MUT}}\right)^{-1} S_{22}^{\mathrm{MUT}} \\ \left(S_{21}^{\mathrm{MUT}}\right)^{-1} S_{11}^{\mathrm{MUT}} & S_{12}^{\mathrm{MUT}} - S_{11}^{\mathrm{MUT}}\left(S_{21}^{\mathrm{MUT}}\right)^{-1} S_{22}^{\mathrm{MUT}} \end{bmatrix} \quad (6)$$

where MUT corrected scattering parameters $\{S_{11}^{\mathrm{MUT}}, S_{21}^{\mathrm{MUT}}\}$ are referenced to interface 1 and $\{S_{22}^{\mathrm{MUT}}, S_{12}^{\mathrm{MUT}}\}$ are referenced to interface 2 (Fig. 1). For the lossless air slab with propagation length of d, $S_{21}^{\mathrm{AIR}} = S_{12}^{\mathrm{AIR}} = e^{-j\beta_0 d}$ and $S_{11}^{\mathrm{AIR}} = S_{22}^{\mathrm{AIR}} = 0$. Therefore, the corrected transfer matrix $\mathbf{Q}^{\mathrm{AIR}}$ can be expressed from the known scattering parameters of the air standard as

$$\mathbf{Q}^{\mathrm{air}} = \begin{bmatrix} e^{j\beta_0 d} & 0 \\ 0 & e^{-j\beta_0 d} \end{bmatrix}. \quad (7)$$

The parameter β_0 is the plane wave propagation constant in air and d is the thickness of the MUT. The transfer matrix for the metallic conductor plane, $\mathbf{Q}^{\mathrm{MCP}}$, diverges since it is assumed that zero power is transmitted through the MCP equivalent to the admittance of a short circuit. However, the scattering parameters of the metallic conductor are finite and can be expressed as $S_{11}^{\mathrm{MCP}} = S_{22}^{\mathrm{MCP}} = -1$ and $S_{21}^{\mathrm{MCP}} = S_{12}^{\mathrm{MCP}} = 0$. The values for the scattering parameters of the MCP are based on the assumption that the conductivity of the MCP reference is much larger than that of MUT, $\sigma_{\mathrm{MCP}} \gg \sigma_{\mathrm{MUT}}$. Unlike [23], we do not calculate the elements of matrices $\mathbf{A}$ and $\mathbf{B}$. But we show in the Appendix that the multiplication of the five matrices in (4) and the knowledge of the scattering parameters of the MCP leads to the following explicit expressions for the corrected scattering parameters S_{11}^{MUT} and S_{21}^{MUT}

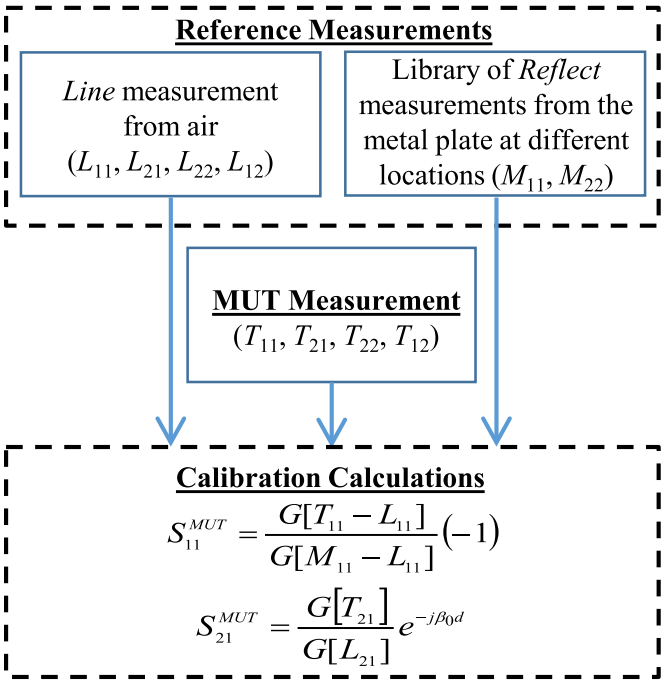

Fig. 2. Summary of the error correction procedure for S_{21}^{MUT} and S_{11}^{MUT}.

(see the Appendix for details):

$$S_{11}^{\mathrm{MUT}} = \frac{G[T_{11} - L_{11}]}{G[M_{11} - L_{11}]}(-1) \tag{8}$$

$$S_{21}^{\mathrm{MUT}} = \frac{G[T_{21}]}{G[L_{21}]} e^{-j\beta_0 d} \tag{9}$$

where again, L_{11}, M_{11}, and T_{11} are the measured scattering parameters corresponding to microwave power reflected from air, MCP, and MUT, respectively. Parameters T_{21} and L_{21} are the measured scattering parameters corresponding to microwave power transmitted through MUT and air, respectively; d is the sample thickness; and β_0 is the plane wave propagation constant in air. The *time gating procedure* G isolates the primary transmission or reflection from the MUT. The gating procedure can be performed by transforming the frequency domain measurements to the time domain using the inverse fast Fourier transform (IFFT). The reflection/transmission from MUT can then be isolated by multiplying the time domain measurement with a Gaussian window centered at the same time instant as the maximum of the first reflection/transmission. The width of the Gaussian window is selected to capture the response from the MUT. The time gating procedure G is detailed in (A4)–(A8). The corrected S_{22}^{MUT} and S_{12}^{MUT} can be obtained from the measured scattering parameters T_{22}, L_{22}, M_{22}, T_{12}, and L_{12} referenced at the interface 2 of the MUT, similar to that described above for interface 1. The entire calibration procedure is summarized in Fig. 2.

For the correction of S_{11}^{MUT} to adequately reflect the specimen characteristic, interface 1 of the specimen and interface 1 of the MCP have to be aligned by locating both interfaces at the same distance (ℓ) from antenna A as shown in Fig. 1. Similar requirements apply to S_{22}^{MUT} at interface 2. If the MCP reference has the same thickness as the MUT, only one MCP location is needed to align the interfaces of the MUT with the MCP as shown in Fig. 1. We can achieve this alignment with an uncertainty of ± 0.1 μm which is the minimum step of the motorized stage that controls the position of the samples. The uncertainty of ± 0.1 μm leads to an uncertainty of ± 2 $\beta_0(0.1\ \mu\mathrm{m}) = \pm 0.012°$ in the phase of S_{11}^{MUT} and S_{22}^{MUT} at 40 GHz whereas it has a negligible effect on the other scattering parameters. This leads to uncertainty in order of $\pm 10^{-5}$ in the reconstructed relative dielectric permittivity which is negligible in comparison to the other uncertainties discussed in Section IV.

However, in most cases, the thickness of the MCP differs from that of the specimen. Then M_{11} and M_{22} are measured separately at interfaces 1 and 2. Scattering parameters of *MCP* can be measured in advance at several different values of ℓ, before measuring the MUT, and stored in a library of calibration data (Fig. 2). In the case when the measurements are performed on an MUT with an arbitrary thickness, the two correct M_{11} and M_{22} data that align with interfaces 1 and 2 can be then re-called from this stored library. We built a library of 200 MCP locations in steps of 50 μm which can accommodate specimens having thicknesses from 50 μm to 9.95 mm. All the MUTs that we tested did not require additional MCP locations. But if the thickness of the MUT required more MCP locations, we can readily add them to the library. Since the *Line* measurement can also be stored in the library, in routine materials evaluation the LR calibration procedure allows the corrected scattering parameters to be obtained from a single measurement of $\{T_{11}, T_{21}, T_{22}, T_{12}\}$ at MUT known location ℓ.

B. Conductivity of Sheet Materials Where $|S_{21}^{MUT}| = |S_{12}^{MUT}| \approx 0$ and $|S_{11}^{MUT}|$, $|S_{22}^{MUT}| > 0.7$

The general complex relative permittivity of an MUT can be expressed as $\varepsilon_r = \varepsilon_r' - j\sigma/(\omega\varepsilon_0)$, where ε_r' is the real part of the complex relative permittivity of the MUT, σ is the conductivity of the MUT, ω is the radial frequency of the incident wave, and ε_0 is the permittivity of free space. A large variety of advanced nanocarbon composite materials can have quite high conductivities such that the reflected wave S_{11}^{MUT} dominates the response while the transmitted wave S_{21}^{MUT} through the specimen is negligibly small or comparable to the noise level in free-space measurements. In other words, for some MUT the conductivity is large enough such that the skin penetration depth is much smaller than the specimen thickness and the conventional transmission-reflection network models cannot be directly applied. Moreover, the conductivity of these highly conducting samples can vary considerably, from 10^2 to 10^4 S/m, and it is important to assess their conductivity quantitatively [32]. To solve that problem, we treat the conductivity of the referenced MCP as an ideal reflector, with infinite conductivity, for which the wave penetration depth $\delta_p \approx 0$. For highly conducting MUT, the conductivity is typically large, $\sigma \gg \omega\varepsilon_0\varepsilon_r'$, such that it dominates the complex relative permittivity of the MUT. Therefore the skin penetration depth can be expressed as $\delta_p = 1/(\pi\, f_0 \mu\, \sigma)^{1/2}$ and the admittance Y_s of such a conducting sheet can be

approximated by [33]

$$Y_s \approx (\sigma \delta_p)/(1+j) = G_s/(1+j) \tag{10}$$

where G_s is the sheet conductance measured in (S). By making use of the expression for Y_s in (10), and noting that after error correction S_{11}^{MUT} is the same as the reflection coefficient for a nontransparent specimen, the relationship between S_{11}^{MUT} and the sheet resistance R_s can be expressed as

$$S_{11}^{\mathrm{MUT}} = \frac{Y_0 - Y_s}{Y_0 + Y_s} \tag{11a}$$

$$S_{11}^{\mathrm{MUT}} = \frac{Y_0 - G_s/(1+j)}{Y_0 + G_s/(1+j)} \tag{11b}$$

$$\left|S_{11}^{\mathrm{MUT}}\right|^2 = \frac{G_s^2 - 2G_sY_0 + 2Y_0^2}{G_s^2 + 2G_sY_0 + 2Y_0^2} \tag{11c}$$

where $Y_0 = 1/120\pi\, S$ is the free space admittance. Solving the quadratic equation (11c) for Y_s yields two σ values

$$\sigma = \pi f_0 \mu_0 G_s^2. \tag{12}$$

Here, the correct value for σ is identified by rejecting the smaller value since it does not correspond to a *microwave-nontransparent* specimen having a thickness d larger than the skin depth (δ_p).

C. Relative Permittivity and Conductivity of Sheet Materials With $S_{21}^{MUT} = S_{12}^{MUT} > 0$ and $|S_{11}^{MUT}|, |S_{22}^{MUT}| < 0.7$

Following the correction procedure, the corrected scattering parameters obtained from (8) and (9) can be used directly as quality indicators in manufacturing or they can be deconvoluted to extract the materials characteristic properties, such as the complex impedance Z_s, reflection coefficient Γ, transmission coefficient τ, and complex propagation constant γ. The relation between the corrected scattering parameters S_{11}^{MUT}, S_{21}^{MUT}, and Z_s, Γ and τ are known [34]–[36] and given by equations

$$\Gamma = b - \sqrt{b^2 - 1}, \quad b = \frac{\left(S_{11}^{\mathrm{MUT}}\right)^2 - \left(S_{21}^{\mathrm{MUT}}\right)^2 + 1}{\left(S_{11}^{\mathrm{MUT}}\right)^2} \tag{13a}$$

$$\tau = \frac{\left(S_{11}^{\mathrm{MUT}}\right)^2 + \left(S_{21}^{\mathrm{MUT}}\right)^2 - \Gamma}{1 - \left(S_{11}^{\mathrm{MUT}} + S_{21}^{\mathrm{MUT}}\right)\Gamma} \tag{13b}$$

$$Z_s = \frac{1+\Gamma}{1-\Gamma}. \tag{13c}$$

The microwave absorption (A), reflection (R), and transmission (T) coefficients can be obtained from the power conservation formula, $A + T + R = 1$, where $T = \tau\tau^*$ and $R = \Gamma\Gamma^*$. The shielding effectiveness (SE) is calculated as a power loss from the reflection and absorption combined [37], [38], $\mathrm{SE} = -10\log\,(1-(R+A))$. The complex dielectric permittivity $\varepsilon_r = \varepsilon_r' - j\sigma/(\omega\varepsilon_0)$ can be obtained from the corrected scattering parameters (8), (9) using a conventional *Transmission-Reflection* model of a passive microwave network and root searching algorithms [25], [36].

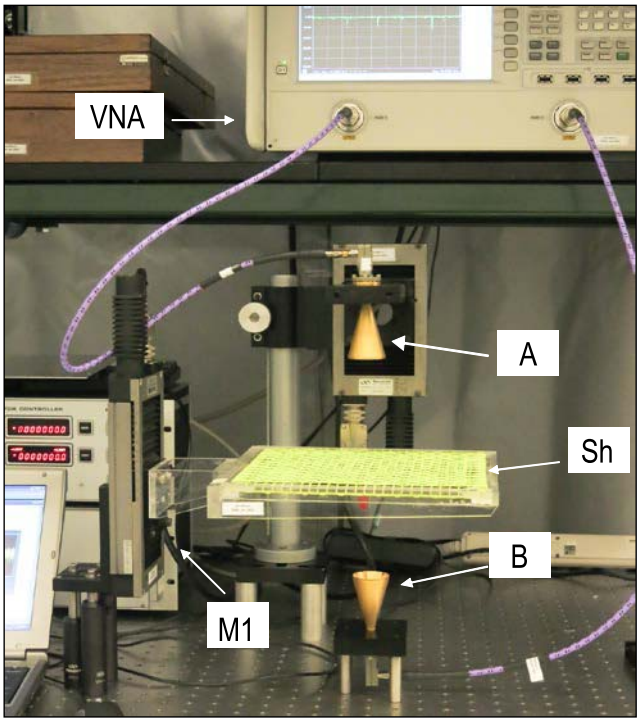

Fig. 3. Experimental setup. Antennas A and B are connected to port 1 of the VNA. Motorized stage M1 positions the specimen holder.

III. Experimental Results

A. Experimental Setup

The noncontact microwave measurement system shown in Fig. 3 utilizes two WR22 conical horn antennas, (from Custom Microwave) to ensure portability and reproducibility of our measurement system in quality control applications. Certain corrugated custom antennas can enhance the signal-to-noise ratio (SNR). However, we verified that the conical antennas we used provided adequate SNR and uncertainty in extracting the characteristics of the MUTs. Specifically, the antennas provide: 1) a voltage standing wave ratio < 1.1 in the Q-band; 2) a gain that varies between 20 and 22 dBi in the Q-band; and 3) a 10-dB beamwidth of 23° and 27° in the E-plane and H-plane, respectively, at the frequency of 41.5 GHz. These specifications are very similar to the specifications of the antennas used in similar high precision free-space systems as reported in [8] and [25].

The conical antennas were connected to a VNA (N5225A from Agilent) via a WR22 waveguide to a 2.4-mm coax transition (Agilent Q281A, B). Our VNA N5225A has been custom configured by Agilent with the option 210. The frequency stability at 10 MHz is better than 1 ppm. The system simultaneously measures scattering parameters of the transmitted and reflected waves in the Q-frequency band (30–50 GHz) centered at 40 GHz. The real part of the relative dielectric permittivity of air in the Q-band is approximately $\varepsilon_r' \approx 1.00058$ [39]–[41]. This corresponds to a wavelength $\lambda_0 \approx 7.493$ mm at the center frequency of 40 GHz. It is worth noting that this wavelength differs by approximately 2 μm from the free space or vacuum wavelength of 7.495 mm.

TABLE I
PERMITTIVITY ε_r' AND CONDUCTIVITY σ OF MUT WITH THE CORRESPONDING UNCERTAINTIES AT 40 GHz

MUT	ε_r'	$(\Delta\varepsilon_r')_s$	$(\Delta\varepsilon_r')_x$	σ (S/m)	$(\Delta\sigma)_s$ (S/m)	$(\Delta\sigma)_x$ (S/m)
PTFE	1.9	0.036	0.02	0.004	0.015	0.02
PMMA	2.4	0.057	0.05	0.034	0.023	0.025
C1	4.5	0.146	0.08	6.3	0.31	0.87
C2	-	-	-	105	14	2.4

$(\Delta\varepsilon_r')_s$ and $(\Delta\sigma)_s$ are the combined uncertainties from uncertainty in the corrected S_{ij} magnitude, $\Delta|S_{ij}|=0.01$, and phase $\Delta\varphi = 1.5°$. $(\Delta\varepsilon_r')_x$ and $(\Delta\sigma)_x$ refer to uncertainty due to mismatch of $x = 250$ μm between the interfaces of the MUT and the metallic reference plate used in calibration.

The distance between antennas is 225 mm ($\sim 30\lambda_0$) and the beam radius at the specimen plane in the middle between antennas is about $7\lambda_0$ which we verified using an absorber with varying aperture in the center. Since CNT composites are typically fabricated as laminates and sheets with a much larger surface area than the beam width, no further confinement of the fields was required. All the specimens tested herein have lateral dimensions of at least 300 mm × 300 mm, or three times larger than the diameter of the beam width, which minimizes surface wave propagation and edge parasitic effects.

Alignment and parallelism verification of the holder plane and the planes of the antennas are performed against a reference chosen as the desk plane on which the entire set-up is mounted. We employed three axis triangulation with commercially available laser pointers. The frame of the specimen holder is a 295 mm × 295 mm square. The maximum tilt of the holder plane measured along the three sides from the reference corner is ±0.5 mm (0.11°). The typical deviation from the planarity along the diagonal, due to temperature variation and specimen load is, ±0.05°. The parallelism of the aluminum MCP is similar or better than that specified above and its surface roughness is in the range of 0.4–0.8 μm. This tilting, surface roughness, as well as other factors, can lead to an alignment mismatch between the interfaces of the sample and the interfaces of the reference MCP used in calibration. The effect of this misalignment mismatch on the reconstructed complex dielectric permittivity is shown in Table I and the uncertainty analysis is detailed in Section V.

The system is initially calibrated with the Short, Open and Load standards at the coax ends. The final calibration procedure, which removes the background reflections and internal reflections due to residual impedance mismatch of the antennas to the free-space transition, was described in the previous section. The magnitude and phase of the microwave scattering parameters can then be accurately determined at the specimen surface for extraction of the material characteristics. As an MCP reflection reference, we used a flat aluminum sheet, 300 mm × 300 mm having a thickness of 1.0 mm ± 0.05 mm and conductivity of 2.3×10^7 S/m. To build a library of MCP positions, after each frequency scan the MCP is moved from the initial position toward antenna A (Fig. 1) in equal steps $\Delta x = 50\ \mu\text{m} \pm 0.1\ \mu\text{m}$, each step being a fraction of the specimen thickness, while the antennas remain fixed at the calibration position. A total of 200 different MCP locations, in steps of 50 μm, are collected in this paper.

CNT composites are typically fabricated as laminates and sheets with large surface areas (>300 mm × 300 mm). Therefore, the main goal of this paper is to develop an NDE technique for composites with similarly large surface areas. For an accurate assessment of the experimental measurements, the samples used for characterization need to be similar in size to typical CNT composites. It is extremely challenging to find inexpensive and homogeneous conductive samples, such as graphene, with areas larger than 300 mm × 300 mm [7]. The dielectric properties of poly(methyl methacrylate) (PMMA) and polytetrafluoroethylene (PTFE) are well known and they are readily available from many commercial sources with large surface areas, customizable shape, and electronic high quality grades. Therefore, we used commercial PMMA and PTFE samples as inexpensive and convenient verification specimens. The thickness of the PTFE specimen is 1.70 mm, while the PMMA specimen has a thickness of about 1.95 mm. The relative dielectric permittivity, ε_r of PTFE and PMMA is known to be approximately $1.9 - j10^{-4}$ [42] and $2.4 - j0.015$ [43], [44], respectively.

Microwave absorbing and reflecting carbon nanostructured composites (CNSs), were also obtained from commercial sources. These advanced multilayer thin film epoxy composites with interlaminar carbon nanostructures are electrically conductive. During manufacturing, the conductivity of CNS materials evolves, as a function of nanocarbon concentration, from a nonconducting dielectric through a conductivity percolation transition until the desired properties are obtained. The two composite materials contain a similar amount of nanocarbon, about 9% by mass, of highly conducting MWCNT network, but they differ in their laminar construction. Composite C1 is reinforced with T300 carbon fabric and glass-fabric modified with MWCNTs and is nominally 2.0 mm ± 0.05 mm thick. Composite C2 contains glass-fabric modified with MWCNTs and its nominal thickness is 1.0 mm ± 0.05 mm. The final product may have conductivity properties similar to that of a metal. Such changes in properties can be accurately captured by measuring the magnitude and phase of the scattering parameters in the microwaves as illustrated in Fig. 4.

B. Scattering Parameters and Materials Characteristics

Fig. 4(a) and (b) shows the magnitude and phase, respectively, of the corrected experimental scattering parameter S_{21}^{MUT} for PTFE and PMMA dielectrics and two representative nanocarbon epoxy-laminate composites C1 and C2. Fig. 4(c) and (d) shows the magnitude and phase, respectively, of the corrected experimental scattering parameter S_{11}^{MUT} for the previously mentioned four MUT. In each of the four figures [Fig. 4(a)–(d)], the label 1 refers to PTFE, label 2 refers to PMMA, label 3 refers to C1, and label 4 refers C4. Both PTFE and PMMA have comparable thicknesses and a relatively small permittivity compared to that of free space. Thus, these dielectric specimens show small reflection with

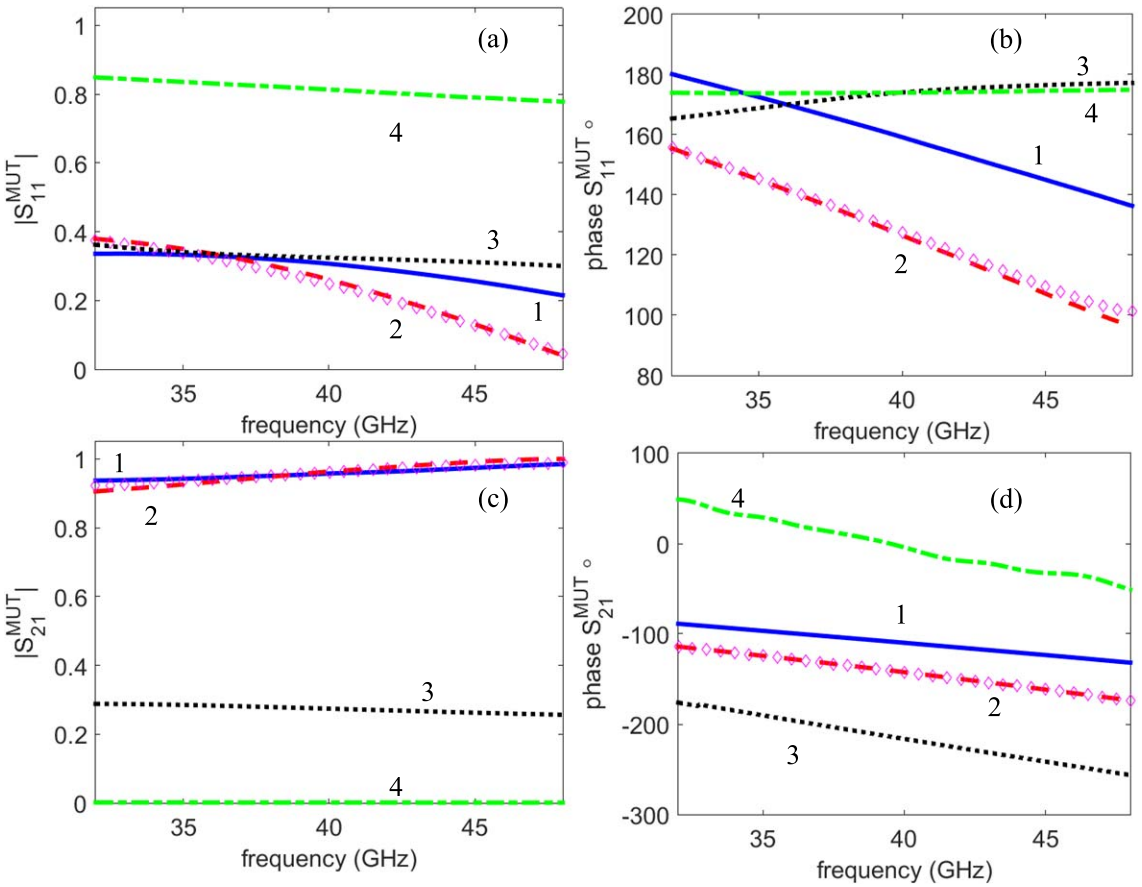

Fig. 4. (a) Magnitude and (b) phase of the corrected S_{11}^{MUT}. (c) Magnitude and (d) phase of the corrected S_{21}^{MUT} for the following specimens. 1—PTFE. 2—PMMA. 3—composite C1. 4—composite C2. Symbols (◊) represent calculated S parameters for PMMA assuming complex permittivity $\varepsilon_r = 2.4 - j0.015$.

magnitude of S_{11}^{MUT} in the range of 0.4 (−10 dB) and relatively large transmission with magnitude of S_{21}^{MUT} in the range of 0.9 (−0.9 dB). The phase of S_{21}^{MUT} for both PTFE and PMMA decrease with frequency as anticipated due to electrical delay in propagation that is proportional to the permittivity and the thickness of the specimens and inversely proportional to the wavelength. The phase change of S_{21}^{MUT} is 44° for PTFE and 59° for PMMA. The phase delay in S_{21}^{MUT} of the PMMA specimen is larger than that for PTFE primarily due to larger real part of the complex permittivity. The diamond symbols, shown in label 2 of Fig. 4(a)–(d), illustrate the calculated scattering parameters for PMMA using the Nicolson-Ross *Transmission-Reflection* model [34] and $\varepsilon_r = 2.4 - j0.015$. It is seen in Fig. 4 that the calculated scattering parameters agree well with experiment indicating the overall appropriateness of our correction procedure in Section III. The calculated results also explain that the apparent decreases of $|S_{11}^{\mathrm{MUT}}|$ seen in Fig. 4 for PMMA only, which results from a half wavelength minimum in reflection at approximately 50 GHz.

In comparison to the dielectrics MUTs, PTFE, and PMMA, the corrected scattering parameters of the composites materials are distinctly different. The two composite materials contain a similar amount, about 9% by mass, of highly conducting MWCNT network, but they differ in their laminar construction. According to Fig. 4(a)–(d) (labels 3 and 4), the differences in construction have a profound effect on the microwave response. For C1 at the center frequency of 40 GHz $|S_{11}^{\mathrm{MUT}}|$, which quantifies the reflected microwave power, is about 0.32 and $|S_{21}^{\mathrm{MUT}}|$, which quantifies the transmitted microwave power, is about 0.27. From relations (13), one can find that at 40 GHz the reflection coefficient (R) of C1 is 0.10, the transmission coefficient (T) is about 0.073 and the resulting absorption coefficient (A) is about 0.827. Thus composite C1 absorbs 82.7% of the incident radiation. The conductivity of composite C1 at 40 GHz is about 6.3 S/m (see Fig. 5 and Table I). In comparison, composite C2 is much more reflecting, and transmits considerably less microwave power than C1. In the case of composite C2, the magnitude of $|S_{11}^{\mathrm{MUT}}|$, is quite large, in the range of 0.81 at 40 GHz. The magnitude of the corresponding scattering parameter $|S_{21}^{\mathrm{MUT}}|$ is significantly smaller, about 0.001, and consequently, the SE of C2 is relatively large, SE ≈ 60 dB at 40 GHz. Such a large SE value can be achieved if the microwave skin penetration depth δ_p is considerably smaller than the specimen thickness d, i.e., $\delta_p = 250\ \mu\mathrm{m} < d = 1$ mm, T is small and the reflection loss R is large. Such a response is characteristic of highly conducting materials, which reflect back most of the incident microwave radiation with phase angle of about 180°. Indeed, the conductivity of composite C2 is about 105 S/m, approximately 20 times larger than that

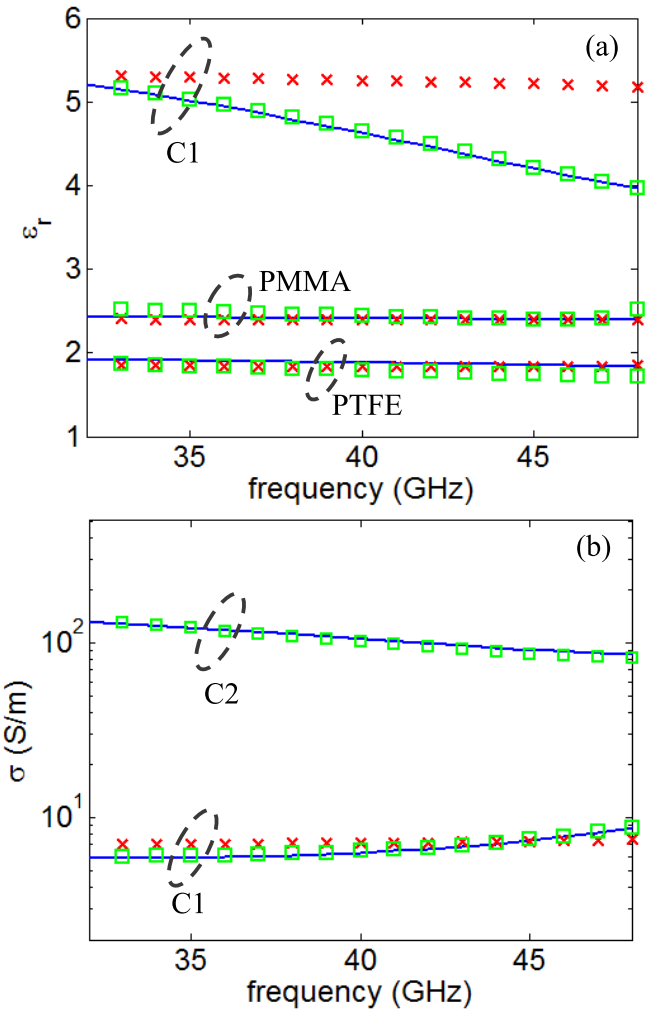

Fig. 5. (a) Real part of the complex relative dielectric permittivity measured for PTFE, PMMA, and CNT composite C1. (b) Conductivity of composites C1 and C2. Lines denote LR correction procedure. Symbols denote the following error correction procedure: LNN/LRR (□) and simplified Ls (×).

of composite C1 (Fig. 5). As already inferred from the scattering parameters, composite C2 shows predominantly metallic reflectivity. At 40 GHz, the composite C2 reflects about 66% ($R = 0.661$) of incident microwave power due to its conductivity. What is not immediately apparent from the scattering parameters shown in Fig. 4 (label 4), is that C2 also absorbs about 34% ($A = 0.338$) of incident radiation due to electric field attenuation and the corresponding resistive losses. The dielectric and conductivity properties of the tested materials are summarized in Table I.

C. Comparison of LR Correction Models With the Line-Network-Network Method

As already indicated, the LNN and LRR require reference measurements from three specimen locations but do not utilize the MCP reflection reference [25], [26]. Therefore, we employed LNN as an independent method to validate our LR error-correction model for specimen with $|S_{21}^{\mathrm{MUT}}|$ and $|S_{12}^{\mathrm{MUT}}| > 10^{-3}$ and we used the LRR to validate our LR error-correction model for specimen with $|S_{21}^{\mathrm{MUT}}|$ and $|S_{12}^{\mathrm{MUT}}| \approx 10^{-3}$. Performing the LRR and LNN procedures, we measured the scattering parameters at three specimen locations, separated by an equal shift of $\Delta x = 1500\ \mu$m. Choosing different values of Δx yielded similar correction results. In addition to LR, we also explored a simplified error correction (Ls) using only the transmittance scattering parameters S_{21}^{MUT}, S_{12}^{MUT} while neglecting reflections S_{11}^{MUT}, S_{22}^{MUT} and, therefore, omitting reference reflection from MCP, i.e., the *Reflect* calibration step. Such simplified correction can produce results comparable to that of LR and LNN when the magnitude of S_{21}^{MUT} and $S_{12}^{\mathrm{MUT}} > 0.5$ (–6 dB).

Fig. 5(a) compares the reconstructed real part of permittivity for PTFE, PMME and composite C1 obtained using the LNN and LR models. It is seen that our LR correction model compares well with the LNN results. The real part of the permittivity of PTFE, PMMA, and the composite C1 obtained either through LNN correction or LR correction agrees to within 1%. The simplified Ls correction result in similarly small deviation for PTFE and PMMA, for which $S_{21}^{\mathrm{MUT}} \cong 0.9$ (-1 dB) [Fig. 5(a)]. However, Fig. 5(a) indicates that in the case of composite C1, the difference between LR or LNN and Ls increases with frequency and approaches about 8% at 40 GHz, where the magnitude of $S_{21}^{\mathrm{MUT}}$is about 0.3 (-10 dB). The simplified Ls can provide satisfactory results to within 5% as long as the magnitude $S_{21}^{\mathrm{MUT}} > 0.5$ (-6 dB). Thus it can be a fast, practical, and convenient solution for MUT with relatively small conductivity and low absorption. The fact that the Ls corrected scattering parameters do not depend on the position of the specimen between antennas is probably the most attractive aspect of the Ls correction. The measurement results obtained with different correction procedures are illustrated in Fig. 5.

Fig. 5(b) compares the conductivity of composites C1 and C2. Due to the large conductivity of C2, S_{21}^{MUT} is only about 0.001 (-60 dB), too small for LNN, we implemented LRR error correction model instead, to verify our LR error correction model and (8) and (9). Again, the conductivity of composites C1 and C2 obtained through LRR correction agrees well, to within 1%, with the LR correction. Similar to the LRR, our proposed calibration employs transmission through air as the Line reference. However, the LRR calibration requires two reflections from two different locations of the specimen being tested. In our approach, we just used one reflection from the MCP as a reference. Thus our method is distinctly different from LRR and, in particular, it does not require the movement of the specimen or the antennas. Thus, the results shown in Fig. 5 reaffirm that the presented LR error correction model and the measurement procedure can be used to reliably determine the conductivity and permittivity of materials whether they are *microwave-transparent* or *microwave-nontransparent*. This system has the potential to act as a scanner to map the conductivity at different locations of a CNT composite.

IV. Uncertainty Analysis

Several uncertainty factors such as instrumentation, dimensional uncertainty of the test specimen geometry, and roughness and geometrical imperfections of the specimen surfaces

contribute to the combined uncertainty of the measurements. Adequate analysis can be performed, however, using the partial derivative technique [45] and considering the instrumentation and the dimensional errors. The standard uncertainty of S_{ij} can be assumed to be within the manufacturer's specification for the network analyzer, about $\pm$ 0.0005 for the magnitude and $\pm$ 0.5° for the phase. The complexity of modeling these factors is considerably higher within the frequency range, where the ringing due to impedance mismatch between antennas and free space interfere directly with the reflected and transmitted scattering parameters of the MUT. The distance of $30\lambda_0$ that we choose between antennas minimizes spurious reflections while enabling the achievement of considerable improvement in the dynamic range of the scattering parameters. In our experiment, the experimental uncertainty in corrected S_{ij} parameters is typically about $\pm$0.01 for the magnitude and $\pm$ 1.5° for the phase, with the noise level in the range of -65 dB. This leads to relative uncertainty of 1.5% for $\varepsilon_{\mathrm{r}}'$ and 2% for σ.

Several additional factors contribute to the combined uncertainty, which can be estimated considering the contribution from individual error components. One of the largest contributing factors to the combined uncertainty of the permittivity and conductivity is the uncertainty in the distribution of the film thickness, and sagging of the specimen that can lead to an alignment mismatch between the specimen interfaces and the interfaces of the metal plate used in the LR calibration. This affects the corrected values of the complex S_{11}^{MUT} and S_{22}^{MUT} parameters. We note that the values of the complex parameters S_{21}^{MUT} and S_{12}^{MUT} are not affected by this misalignment. Due to the nonlinearity of (8) and (9), the partial derivative method [45] cannot be evaluated analytically. Nevertheless, we estimate quantitatively the misalignment effect by reconstructing permittivity and conductivity using S_{11}^{MUT} and S_{22}^{MUT} determined at several specimen locations separated by Δx

$$\Delta\varepsilon_r' = \varepsilon_r'(\Delta x) - \varepsilon_r'(0) \tag{14}$$

$\varepsilon_r'(\Delta x)$ is the reconstructed real part of the complex relative permittivity when there is a mismatch Δx between the interfaces of the sample and the interfaces of the metal plate and ε_r' (0) is the reconstructed real part of the complex relative permittivity when the metal plate is positioned at the correct location with zero mismatch between the interfaces of the sample and the interfaces of the metal plate. A similar approach was applied to estimate $\Delta\sigma$. We selected Δx to be 50 μm, which is the step we used to build the collection of the MCP reference measurements. Smaller Δx did not lead to any significant improvement in the combined uncertainty. Typically, uncertainty from LR in the reconstructed value of the dimensionless ε_r' is of the order of 0.1 and uncertainty in σ is in the range of 0.5 S/m per every 50 μm of mismatch. The uncertainty in (14) does not exhibit any specific pattern with respect to the frequency or the permittivity of the specimen, but it can be assumed to increase linearly with Δx within $\pm$ 250 μm of mismatch. Table I summarizes these results.

All the measurements were obtained in our laboratory at ambient conditions with nominal relative humidity (RH) of 50% $\pm$ 10% and temperature (T) of 293 K $\pm$ 1%. At these nominal conditions, the amount of water in air is about 8.6 g/m^3 of air or 1.45×10^{-2} mole fraction ($\mathrm{mol}_{H_2O}/\mathrm{mol}_{\mathrm{air}}$). The corresponding relative dielectric constant of humid air $\varepsilon_r' = 1.000580$ [39]. We note that in the definition of the matrices $\mathbf{Q}^{\mathrm{air}}$ we neglected the real part of the propagation constant α, which represents the attenuation due to the dielectric loss from the moisture in humid air. This simplification is justified since at 35 GHz the attenuation coefficient of humid air $\alpha \approx 10^{-4}$ dB/m ($\alpha \approx 1.15 \times 10^{-5}$ Np/m) [40]. Evidently, the attenuation due to moisture in air at the nominal temperature−humidity conditions is too small to make a noticeable effect on our results.

To assess the uncertainty in the scattering parameters due to variations in the moisture content in more detail, we consider the case where at the temperature of 290 K, the humidity increases from 25% to 75%, which encompasses a range of conditions well beyond their possible variations in our laboratory. From the data in [39], we find that at RH of 75% the mole fraction of water increases to about 1.7×10^{-2}, yet the change in ε_r' is not significant, $\varepsilon_r' \approx 1.000582$. The attenuation coefficient at 35 GHz increases from 6×10^{-5} to 1.5×10^{-4} dB/m [40]. The distance between the transmitting and receiving antennas in our experimental setup is 225 mm. Therefore, this change in the attenuation coefficient corresponds to uncertainty of the order of $\pm 2.025 \times 10^{-5}$ dB. Similarly, if the RH is constant at 75% and the temperature varies from 280 to 310 K, the attenuation coefficient increases from 9×10^{-5} to 2.7×10^{-4} dB/m, which corresponds to an uncertainty of $\pm 4 \times 10^{-5}$ dB. Thus, the possible variations in temperature and humidity in the lab environment can lead to uncertainties in the order of $\pm 10^{-5}$ dB in the magnitude of the measured scattering parameters which can be neglected with respect to the other uncertainties quantified in Table I. Regarding the phase constant in air, [39]–[41] show that in the *Q*-band frequency range, the phase constant for air varies slightly with temperature and humidity, between 1.00025 and 1.00035 ω/c_0. This leads to an uncertainty of 0.0001 $\omega/c_0 \times$ (225×10^{-3} m) radians in the phase of the scattering parameters, which corresponds to a maximum uncertainty of 0.0236 radians or 1.35° in the phase of the measured scattering parameters at a frequency of 50 GHz. This uncertainty is comparable to the uncertainty presented in Table I.

The above analysis shows that, in the indicated range of temperature and humidity conditions, the moisture in air has an insignificant effect on the uncertainty of the measured scattering parameters. Additional analysis may be required, however, if the proposed technique is employed in more extreme environments when, for example, the temperature increases by more than 30 K from the ambient conditions or RH approaches a saturation of 100%. Also, for long-term measurements performed over a period exceeding several months, the reference measurements may need to be refreshed periodically to minimize any drift noise caused by the drift of the measurement instrumentation [46].

V. Conclusion

We have demonstrated the LR error-correction model and its experimental implementation for broadband noncontact

nondestructive characterization of conducting nanocarbon composites in free space. Our error correction procedure implements a fixed wave propagation distance between antennas. The measurement of the complex scattering parameters is referenced to two standards, *Line* and *Reflect*. The *Line* reference is implemented as an *air slab* having geometrical propagation length equal to that of the specimen under test. The second reference, *Reflect*, involves reflection measurement from a known *metallic conductor*, such as an aluminum plate. The experimental measurements were performed, in the Q-band frequency range of 30–50 GHz, from sheet specimens of PTFE and PMME dielectrics and conducting nanocarbon composite laminates that can be either thicker or thinner than the skin penetration depth. We show that the LR error correction procedure is sufficient to reconstruct materials' properties without ambiguity. The scattering parameters from 1.0-mm-thick aluminum plate were measured at 200 different locations in steps of 50 μm spanning a distance of $\pm$ 5 mm from the center location between the two antennas. Such a collection of reference data provides great flexibility in correcting the scattering parameters of specimens with a wide variety of thicknesses. In effect, in routine materials evaluation LR allows the corrected scattering parameters S_{11}^{MUT} and S_{21}^{MUT}, and S_{12}^{MUT} and S_{22}^{MUT} to be obtained from a single measurement of *mut* $\{T_{11}, T_{21}, T_{22}, T_{12}\}$ located at arbitrary distances from the antennas. The simplicity of the technique makes it attractive for noncontact, nondestructive testing and quality control in the manufacturing environment.

APPENDIX

The expressions for the corrected transmission S_{21}^{MUT} and the corrected reflection S_{11}^{MUT} from the MUT presented in (8) and (9) can be proved by the multiplication of the five matrices in (4). The first element of the transfer matrix $\mathbf{P}^{\mathrm{MUT}}$, p_{11}^{MUT}, can be expressed as follows:

$$p_{11}^{\mathrm{MUT}} = T_{21}^{-1} = k^2 A_{11} q_{11} B_{11} \times \left(1 + \frac{k^{-2}(A_{12}q_{21}B_{11} + A_{11}q_{12}B_{21}) + k^{-4}A_{12}q_{22}B_{21}}{A_{11}q_{11}B_{11}}\right). \tag{A1}$$

Therefore, from (4) the measured T_{21} can be expressed as

$$T_{21} = \frac{k^{-2}}{A_{11}q_{11}B_{11}} \times \left(1 + \frac{k^{-2}(A_{12}q_{21}B_{11} + A_{11}q_{12}B_{21}) + k^{-4}A_{12}q_{22}B_{21}}{A_{11}q_{11}B_{11}}\right)^{-1}. \tag{A2}$$

The antennas are designed such that they transmit/receive most of the input/received power. Therefore, the transfer matrix elements $A_{12}/A_{11} \ll 1$, $A_{21}/A_{11} \ll 1$, $B_{12}/B_{11} \ll 1$, and $B_{21}/B_{11} \ll 1$. Using this condition and expanding the inverse in (A2) as an infinite series, T_{21} can be expressed as

$$T_{21} = \frac{k^{-2}}{A_{11}q_{11}B_{11}} \times \left(1 - \frac{k^{-2}(A_{12}q_{21}B_{11} + A_{11}q_{12}B_{21}) + k^{-4}A_{12}q_{22}B_{21}}{A_{11}q_{11}B_{11}} + O(k^{-4})\right). \tag{A3}$$

The series in (A3) shows explicitly the multiple reflections with the different powers of k indicating the delay required by each multiple reflection to reach antenna B. In order to isolate the first transmission that reaches the receiving antenna B, time gating is applied to isolate only the terms with the power k^{-2} to yield

$$G[T_{21}] = \frac{k^{-2}}{A_{11}q_{11}B_{11}} \tag{A4}$$

where G refers to time gating. The gating is performed by transforming the measurements to the time domain using IFFT. The first reflection/transmission is then isolated by multiplying the time-domain measurement with a Gaussian window as shown in Fig. 6. The maximum of the Gaussian window is positioned at the same location as the maximum of the first reflection/transmission. Typically, the first reflection/transmission is significantly larger than the spurious multiple reflections. The width of the Gaussian window is chosen to reject any spurious multiple reflections/transmissions between the antennas and the MUT as shown in Fig. 6. This width depends on the separation between the antennas and the sample but once the experimental system is established, the width of the Gaussian wave is fixed for the gating of all the measurements. The advantage of the time gating approach is that it employs simple signal processing techniques and its disadvantage is that it can distort the measurements toward the beginning and end of the spectrum and can reduce the resolution in the frequency domain [25], [47]. Since no sharp resonances are anticipated in the CNT composites considered herein and to keep the calibration as simple as possible, time gating was used. Also, only results from 32 to 48 GHz were investigated to avoid the distortions

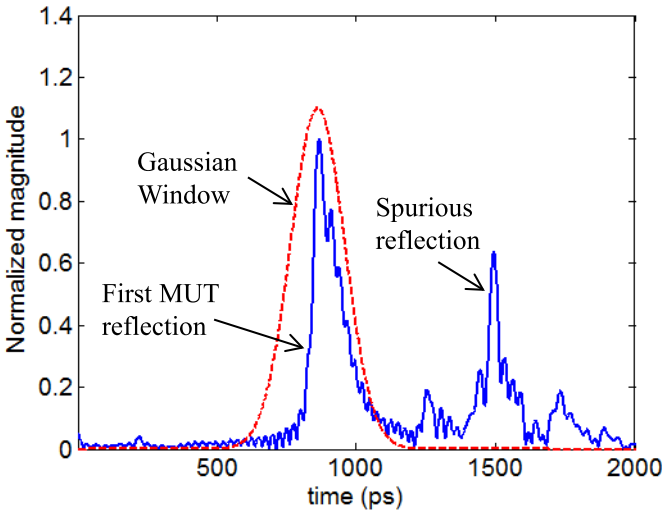

Fig. 6. Time-domain gating procedure.

caused by the time gating at the beginning and end of the spectrum.

If the MUT is removed, the target now consists of an air slab of thickness d, which yields the transfer matrix given in (2). Therefore, for air the measured p_{11}^{air} can be expressed by the multiplication of the five matrices in (2), as follows:

$$p_{11}^{\text{air}} = L_{21}^{-1} = k^2 A_{11}(e^{j\beta_0 d}) B_{11}\left(1+\frac{k^{-4}A_{12}B_{21}(e^{-j2\beta_0 d})}{A_{11}B_{11}}\right). \tag{A5}$$

We invert (A5) and expand the inverse into an infinite series

$$L_{21} = \frac{k^{-2}(e^{-j\beta_0 d})}{A_{11}B_{11}}\begin{pmatrix} 1-\frac{k^{-4}A_{12}B_{21}(e^{-j2\beta_0 d})}{A_{11}B_{11}} \\ +O(k^{-8}) \end{pmatrix}. \tag{A6}$$

Time gating is then applied to isolate only the k^{-2} term to yield

$$G[L_{21}] = \frac{k^{-2}e^{-j\beta_0 d}}{A_{11}B_{11}}. \tag{A7}$$

By combining (A4) and (A7), the corrected transmission through the MUT, S_{21}^{MUT}, referred to interface 2 can be expressed as follows:

$$\frac{G[T_{21}]}{G[L_{21}]}e^{-j\beta_0 d} = \frac{1}{q_{11}} = S_{21}^{\text{MUT}}. \tag{A8}$$

Hence, (8) is proved.

To calibrate the reflection from the MUT, the measured T_{11} can be expressed in terms of the transfer matrix elements as follows:

$$\begin{aligned} T_{11} = \frac{p_{21}^{\text{MUT}}}{p_{11}^{\text{MUT}}} &= \frac{A_{21}}{A_{11}} \\ &\times\left(1+\frac{k^{-2}}{A_{21}q_{11}B_{11}}(A_{22}q_{21}B_{11}+A_{21}q_{12}B_{21}) \right. \\ &\left. +\frac{k^{-4}A_{22}q_{12}B_{21}}{A_{21}q_{11}B_{11}}\right) \\ &\times\left(1+\frac{k^{-2}}{A_{11}q_{11}B_{11}}(A_{12}q_{21}B_{11}+A_{11}q_{12}B_{22}) \right. \\ &\left. +\frac{k^{-4}A_{12}q_{22}B_{21}}{A_{11}q_{11}B_{11}}\right)^{-1}. \end{aligned} \tag{A9}$$

Similar to (A3), the inverse term in (A9) can be expressed as the following infinite series:

$$\begin{aligned} T_{11} &= \frac{A_{21}}{A_{11}} \\ &\times\left(1+\frac{k^{-2}}{A_{21}q_{11}B_{11}}(A_{22}q_{21}B_{11}+A_{21}q_{12}B_{21}) \right. \\ &\left. +\frac{k^{-4}A_{22}q_{12}B_{21}}{A_{21}q_{11}B_{11}}\right) \\ &\times\left(1-\frac{k^{-2}}{A_{11}q_{11}B_{11}}(A_{12}q_{21}B_{11}+A_{11}q_{12}B_{22})+O(k^{-4})\right). \end{aligned} \tag{A10}$$

The time gating of (A10) to isolate the k^{-2} term that corresponds to the first reflection from the sample simplifies the equation to

$$T_{11} = \frac{A_{21}}{A_{11}}\left(1+\frac{k^{-2}q_{21}}{q_{11}}\left(\frac{A_{22}}{A_{21}}-\frac{A_{12}}{A_{11}}\right)+O(k^{-4})\right). \tag{A11}$$

In (A11), the time-gating window is set to extract the first reflection from the MUT that occurs at approximately 900 ps as shown in Fig. 6. The calibration previously reported in [23] is independent of our LR calibration because it uses time gating to isolate the earlier reflection that occurs due to the mismatch between the cable and the antenna. This earlier reflection occurs at approximately 250 ps in Fig. 6. Using an approach similar to (A11), the measured reflection from air can be expressed as

$$L_{11} = \frac{A_{21}}{A_{11}}(1+O(k^{-4})). \tag{A12}$$

By simple signal flow analysis, the measured reflection from the *metal conductor plate* can be expressed as

$$M_{11} = \frac{A_{21}}{A_{11}} - \frac{(A_{22}A_{11}-A_{21}A_{12})k^{-2}}{A_{11}^2 - A_{11}A_{12}k^{-2}}. \tag{A13}$$

By expanding the inverse in the second term in (A13) into an infinite series, it can be simplified to

$$M_{11} = \frac{A_{21}}{A_{11}} - k^{-2}\left(\frac{A_{22}}{A_{11}}-\frac{A_{12}A_{21}}{A_{11}^2}\right)+O(k^{-4}). \tag{A14}$$

By first subtracting L_{11} from both T_{11} and M_{11} and then performing time gating to isolate only the first reflection received by antenna A, which corresponds to the k^{-2} terms, we achieve

$$G[T_{11}-L_{11}] = k^{-2}\frac{q_{21}}{q_{11}}\left(\frac{A_{22}}{A_{11}}-\frac{A_{12}A_{21}}{A_{11}^2}\right) \tag{A15}$$

$$G[M_{11}-L_{11}] = -k^{-2}\left(\frac{A_{22}}{A_{11}}-\frac{A_{12}A_{21}}{A_{11}^2}\right). \tag{A16}$$

Finally, by dividing (A15) by (A16), the corrected reflection at interface 1 of the MUT, S_{11}^{MUT}, can be expressed as follows:

$$\frac{G[T_{11}-L_{11}]}{G[M_{11}-L_{11}]}(-1) = \frac{q_{21}}{q_{11}} = S_{11}^{\text{MUT}}. \tag{A17}$$

Hence, (9) is proved.

ACKNOWLEDGMENT

This paper is an official contribution of the National Institute of Standards and Technology (NIST), not subject to copyright in the U.S. Certain commercial equipment, instruments, or materials are identified in this paper to foster understanding. Such identification does not imply recommendation or endorsement by the NIST, nor does it imply that the materials or equipment identified are necessarily the best available for the purpose.

REFERENCES

[1] M. F. L. De Volder, S. H. Tawfick, R. H. Baughman, and A. J. Hart, "Carbon nanotubes: Present and future commercial applications," *Science*, vol. 339, no. 6119, pp. 535–539, 2013.

[2] H. Yoon, M. Yamashita, S. Ata, D. N. Futaba, T. Yamada, and K. Hata, "Controlling exfoliation in order to minimize damage during dispersion of long SWCNTs for advanced composites," *Sci. Rep.*, vol. 4, pp. 3907–3915, Jan. 2014.

[3] P.-C. Maa, N. A. Siddiqui, G. Marom, and J.-K. Kim, "Dispersion and functionalization of carbon nanotubes for polymer-based nanocomposites: A review," *Compos. A, Appl. Sci. Manuf.*, vol. 41, no. 10, pp. 1345–1367, 2010.

[4] A. M. Hassan and E. J. Garboczi, "Electromagnetic scattering from randomly-centered parallel single-walled carbon nanotubes embedded in a dielectric slab," *IEEE Trans. Antennas Propag.*, vol. 62, no. 10, pp. 5230–5241, Oct. 2014.

[5] N. D. Orloff *et al.*, "Noncontact conductivity and dielectric measurement for high throughput roll-to-roll nanomanufacturing," *Sci. Rep.*, vol. 5, Nov. 2015, Art. no. 17019.

[6] J. Obrzut, C. Emiroglu, O. Kirillov, Y. Yang, and R. E. Elmquist, "Surface conductance of graphene from non-contact resonant cavity," *Measurement*, vol. 87, pp. 146–151, Jun. 2016.

[7] F. C. Smith, B. Chambers, and J. C. Bennett, "Methodology for accurate free-space characterisation of radar absorbing materials," *Proc. Inst. Elect. Eng.—Sci., Meas., Technol.*, vol. 141, no. 6, pp. 538–546, 1994.

[8] D. K. Ghodgaonkar, V. V. Varadan, and V. K. Varadan, "Free-space measurement of complex permittivity and complex permeability of magnetic materials at microwave frequencies," *IEEE Trans. Instrum. Meas.*, vol. 39, no. 2, pp. 387–394, Apr. 1990.

[9] M. H. Umari, D. K. Ghodgaonkar, V. V. Varadan, and V. K. Varadan, "A free-space bistatic calibration technique for the measurement of parallel and perpendicular reflection coefficients of planar samples," *IEEE Trans. Instrum. Meas.*, vol. 40, no. 1, pp. 19–24, Feb. 1991.

[10] V. V. Varadan, R. D. Hollinger, D. K. Ghodgaonkar, and V. K. Varadan, "Free-space, broadband measurements of high-temperature, complex dielectric properties at microwave frequencies," *IEEE Trans. Instrum. Meas.*, vol. 40, no. 5, pp. 842–846, Oct. 1991.

[11] D. Lemaire, D. Cros, H. Jallageas, and P. Guillon, "Material characterisation from −160 °C up to 800 °C in centimeter and millimeter wavelength frequency band," in *Conf. Precis. Electromagn. Meas. Dig.*, 1996, pp. 72–73.

[12] S. Chen, K. A. Korolev, J. Kupershmidt, K. Nguyen, and M. N. Afsar, "High-resolution high-power quasi-optical free-space spectrometer for dielectric and magnetic measurements in millimeter waves," *IEEE Trans. Instrum. Meas.*, vol. 58, no. 8, pp. 2671–2678, Aug. 2009.

[13] G. L. Friedsam and E. M. Biebl, "A broadband free-space dielectric properties measurement system at millimeter wavelengths," in *Conf. Precis. Electromagn. Meas. Dig.*, 1996, pp. 210–211.

[14] G. L. Friedsam and E. M. Biebl, "A broadband free-space dielectric properties measurement system at millimeter wavelengths," *IEEE Trans. Instrum. Meas.*, vol. 46, no. 2, pp. 515–518, Apr. 1997.

[15] H. P. Tran, F. Gumbmann, J. Weinzierl, and L.-P. Schmidt, "Spatial resolution of millimeter wave imaging at 75-100 GHz and 600 GHz," in *Proc. German Microw. Conf.*, 2006, pp. 1–5.

[16] S. Sano, A. Tsuzuki, K. Oda, T. Ueno, Y. Makino, and S. Miyake, "Millimeter wave spectroscopy of alumina-zirconia system," in *Advances in Microwave and Radio Frequency Processing*. Heidelberg, Germany: Springer, 2006, pp. 149–154.

[17] D. Bourreau, A. Péden, and S. Le Maguer, "A quasi-optical free-space measurement setup without time-domain gating for material characterization in the W-band," *IEEE Trans. Instrum. Meas.*, vol. 55, no. 6, pp. 2022–2028, Dec. 2006.

[18] Y. Konishi, M. Kamegawa, M. Case, R. Yu, S. T. Allen, and M. J. W. Rodwell, "A broadband free-space millimeter-wave vector transmission measurement system," *IEEE Trans. Microw. Theory Techn.*, vol. 42, no. 7, pp. 1131–1139, Jul. 1994.

[19] P. Goy and M. Gross, "Free space vector transmission-reflection from 18 to 760 GHz," in *Proc. 24th Eur. Microw. Conf.*, Cannes, France, 1994, pp. 1973–1978.

[20] T. Tosaka, K. Fujii, K. Fukunaga, and A. Kasamatsu, "Development of complex relative permittivity measurement system based on free-space in 220–330-GHz range," *IEEE Trans. THz Sci. Technol.*, vol. 5, no. 1, pp. 102–109, Jan. 2015.

[21] S. Kim, D. Novotny, J. Gordon, and J. Guerrieri, "A free-space measurement method for the low-loss dielectric characterization without prior need for sample thickness data," *IEEE Trans. Antennas Propag.*, vol. 64, no. 9, pp. 3869–3879, Sep. 2016.

[22] M. Liang and H. Xin, "Microwave to terahertz: Characterization of carbon-based nanomaterials," *IEEE Microw. Mag.*, vol. 15, no. 1, pp. 40–51, Jan./Feb. 2014.

[23] P. G. Bartley, Jr., and S. B. Begley, "Improved free-space S-parameter calibration," in *Proc. IEEE Instrum. Meas. Technol. Conf.*, May 2005, pp. 372–375.

[24] D. V. Blackham, "Free space characterization of materials," in *Proc. Antenna Meas. Techn. Assoc. Symp.*, vol. 15. 1993, pp. 58–60.

[25] C. Orlob, T. Reinecke, E. Denicke, B. Geck, and I. Rolfes, "Compact unfocused antenna setup for X-band free-space dielectric measurements based on line-network-network calibration method," *IEEE Trans. Instrum. Meas.*, vol. 62, no. 7, pp. 1982–1989, Jul. 2013.

[26] I. Rolfes and B. Schiek, "LRR—A self-calibration technique for the calibration of vector network analyzers," *IEEE Trans. Instrum. Meas.*, vol. 52, no. 2, pp. 316–319, Apr. 2003.

[27] A. M. Hassan, J. Obrzut, and E. J. Garboczi, "Free-space reconstruction of the electrical properties of carbon nanotube based composites in the Q-band range," in *Proc. 84th Autom. RF Techn. Group Microw. Meas. Conf.*, Boulder, CO, USA, Dec. 2014, pp. 1–4.

[28] L. F. Chen, C. K. Ong, C. P. Neo, V. V. Varadan, and V. K. Varadan, *Microwave Electronics: Measurement and Materials Characterization*, 1st ed. Hoboken, NJ, USA: Wiley, 2004, pp. 175–205.

[29] J.-M. Le Floch *et al.*, "Cryogenic properties of a diamond sample at microwave frequencies," in *Proc. Int. Conf. Electromagn. Adv. Appl. (ICEAA)*, Sydney, NSW, Australia, 2010, pp. 837–840.

[30] J. A. G. Akkermans, R. van Dijk, and M. H. A. J. Herben, "Millimeter-wave antenna measurement," in *Proc. 37th Eur. Microw. Conf.*, Munich, Germany, Oct. 2007, pp. 83–86.

[31] M. Steer, *Microwave and RF Design: A Systems Approach*, 2nd ed. Raleigh, NC, USA: SciTech Publishing, Aug. 2013.

[32] W. Bauhofer and J. Z. Kovacs, "A review and analysis of electrical percolation in carbon nanotube polymer composites," *Compos. Sci. Technol.*, vol. 69, no. 10, pp. 1486–1498, 2009.

[33] R. C. Hansen and W. T. Pawlewicz, "Effective conductivity and microwave reflectivity of thin metallic films," *IEEE Trans. Microw. Theory Techn.*, vol. MTT-30, no. 11, pp. 2064–2066, Nov. 1982.

[34] A. M. Nicolson and G. F. Ross, "Measurement of the intrinsic properties of materials by time-domain techniques," *IEEE Trans. Instrum. Meas.*, vol. IM-19, no. 4, pp. 377–382, Nov. 1970.

[35] J. Obrzut, "General analysis of microwave network scattering parameters for characterization of thin film materials," *Measurement*, vol. 46, no. 8, pp. 2963–2970, Oct. 2013.

[36] J. Baker-Jarvis, E. J. Vanzura, and W. A. Kissick, "Improved technique for determining complex permittivity with the transmission/reflection method," *IEEE Trans. Microw. Theory Techn.*, vol. 38, no. 8, pp. 1096–1103, Aug. 1990.

[37] R. B. Schulz, V. C. Plantz, and D. R. Brush, "Shielding theory and practice," *IEEE Trans. Electromagn. Compat.*, vol. 30, no. 3, pp. 187–201, Aug. 1988.

[38] A. R. Henn and R. M. Cribb, "Modeling the shielding effectiveness of metallized fabrics," in *Proc. IEEE Int. Symp. Electromagn. Compat.*, Aug. 1992, pp. 283–286.

[39] R. Cuccaro, R. M. Gavioso, G. Benedetto, D. M. Ripa, V. Fernicola, and C. Guianvarc'h, "Microwave determination of water mole fraction in humid gas mixtures," *Int. J. Thermophys.*, vol. 33, no. 8, pp. 1352–1362, 2012.

[40] H. J. Liebe, "An updated model for millimeter wave propagation in moist air," *Radio Sci.*, vol. 20, no. 5, pp. 1069–1089, 1985.

[41] W. C. Stone, "NIST construction automation program report no. 3: Electromagnetic signal attenuation in construction materials," Nat. Inst. Standards Technol., Gaithersburg, MD, USA, Tech. Rep. NISTIR 6055, Oct. 1997.

[42] Z. Abbas, R. D. Pollard, and R. W. Kelsall, "Complex permittivity measurements at Ka-band using rectangular dielectric waveguide," *IEEE Trans. Instrum. Meas.*, vol. 50, no. 5, pp. 1334–1342, Oct. 2001.

[43] Z. Awang, F. A. M. Zaki, N. H. Baba, A. S. Zoolfakar, and R. A. Bakar, "A free-space method for complex permittivity measurement of bulk and thin film dielectrics at microwave frequencies," *Prog. Electromagn. Res. B*, vol. 51, pp. 307–328, May 2013.

[44] P. F. Goldsmith, *Quasioptical Systems: Gaussian Beam Quasioptical Propogation and Applications*. Hoboken, NJ, USA: Wiley, 1998, p. 81.
[45] L. Wang, R. Zhou, and H. Xin, "Microwave (8–50 GHz) characterization of multiwalled carbon nanotube papers using rectangular waveguides," *IEEE Trans. Microw. Theory Techn.*, vol. 56, no. 2, pp. 499–506, Feb. 2008.
[46] A. M. Hassan, M. R. Hajihashemi, M. El-Shenawee, A. Al-Zoubi, and A. A. Kishk, "Drift denoising of experimental TE measurements for imaging 2D PEC cylinders," *IEEE Antennas Wireless Propag. Lett.*, vol. 8, pp. 1218–1222, 2009.
[47] K. M. Hock, "Error correction for diffraction and multiple scattering in free-space microwave measurement of materials," *IEEE Trans. Microw. Theory Techn.*, vol. 54, no. 2, pp. 648–659, Feb. 2006.

Ahmed M. Hassan (S'07–M'12) received the B.Sc. (Hons.) and M.Sc. degrees in electronics and communications engineering from Cairo University, Giza, Egypt, in 2004 and 2006, respectively, and the Ph.D. degree in electrical engineering from the University of Arkansas, Fayetteville, AR, USA, in 2010.

From 2011 to 2012, he was a Post-Doctoral Researcher with the Department of Electrical Engineering, University of Arkansas. From 2012 to 2015, he was a Post-Doctoral Researcher with the National Institute of Standards and Technology (NIST), Gaithersburg, MD, USA. Currently, he is an Assistant Professor with the Computer Science Electrical Engineering Department, University of Missouri–Kansas City, Kansas City, MO, USA. His current research interests include nanoelectromagnetics, bioelectromagnetics, nondestructive evaluation, and experimental microwave and terahertz imaging.

Dr. Hassan was a recipient of the Doctoral Academy Fellowship at the University of Arkansas and the Outstanding Poster Award in the 2014 21st Annual NIST Sigma Xi Postdoctoral Poster Presentation.

Jan Obrzut (A'00–M'03) received the Ph.D. degree in technical sciences from Cracow Polytechnic, Cracow, Poland.

After a post-doctoral appointment with the Polymer Science Department, University of Massachusetts-Ahmerst, Ahmerst, MA, USA, he was a Researcher with the Five College Radio Astronomy Department, Amherst, where he was involved with microwave dielectric waveguides. In 1988, he joined IBM as an Advisory Engineer, where he conducted exploratory work on the application of polymer dielectrics in microelectronics. Since 1997, he has been with the National Institute of Standards and Technology (NIST), Gaithersburg, MD, USA, where he researches dielectric films and hybrid materials for microwave and electronic applications. His current research interests include microwave materials characterization, polymer dielectrics, embedded passive devices, and nanocarbon composites.

Edward J. Garboczi received the B.S. degree in physics (Hons.) and the Ph.D. degree in condensed matter physics (theory) from Michigan State University, East Lansing, MI, USA, in 1980 and 1985, respectively.

From 1985 to 1988, he was a Research Physicist with Armstrong World Industries, Inc., Lancaster, PA, USA. From 1988 to 2014, he was a Physicist, a Group Leader, and finally a fellow with the Materials and Structural Systems Division, National Institute of Standards and Technology (NIST), Gaithersburg, MD, USA. In 2014, he moved to the Division of Applied Chemicals and Materials, NIST Boulder, CO, USA. His current research interests include computational materials science, porous materials, electrical properties of nanocomposites, and 3-D particle shape analysis of a wide range of particles, including gravel, sand, cement, chemical explosives, lunar soil, and metal powder for additive manufacturing.

Dr. Garboczi is a Fellow of the American Concrete Institute (ACI) and the American Ceramic Society (ACerS). He was a recipient of the ACI Robert E. Philleo Award, the ACerS Della Roy Lecture Award, the ACers Edward C. Henry Best Paper Award (Electronics Division), and a Silver Medal from the Department of Commerce for the creation of the Virtual Cement and Concrete Testing Laboratory.